Insights into the direct carbonation of activated lizardite: the identification a poorly reactive amorphous Mg-rich silicate phase

K. Rausis[a,], A. Ćwik[a], I. Casanova[a,b]*

[a]Institute of Energy Technologies and Barcelona Research Center in Multiscale Science and Engineering. Universitat Politècnica de Catalunya - Barcelona Tech. Campus Diagonal-Besòs, C3.11, 08019, Barcelona, Spain

[b]Department of Civil and Environmental Engineering. Universitat Politècnica de Catalunya - Barcelona Tech. Campus Nord, B1, 08034, Barcelona, Spain

ABSTRACT

This work aims to shed light on the yet unanswered question regarding the limited carbonation yield of activated lizardite via direct carbonation. Two amorphous Mg-rich silicate phases were identified upon activation. A rapid and complete carbonation of a highly reactive amorphous silicate phase was observed under moderately low pressure and temperature conditions (50-120ºC, 6 bar). Carbonation of this phase yielded to the formation of carbonates and a Si-rich passivating phase. On the other hand, the other amorphous silicate phase remained unaltered upon carbonation,

* Corresponding author.

E-mail address: kwon.rausis@upc.edu; Phone:+34 934011857

fixing a significant amount of Mg within its disordered structure. The presence of poorly reactive intermediate Mg-rich silicate and Si-rich phases might be responsible for the yet unanswered relatively low carbonation efficiencies obtained via direct carbonation of activated lizardite. These limiting factors are considered to reduce the carbonation yield significantly more than the nucleation of forsterite during thermal activation. Analogous experiments carried with different meta-serpentines yielded the formation of distinct carbonate phases. The different distribution of highly and poorly-reactive amorphous phases among the different activated materials might have played an important role in the accelerated formation of magnesite (which was observed to occur once hydromagnesite formation reached a steady state) and the transformation of nesquehonite to dypingite-like phases.

KEYWORDS

Mineral carbonation; activated serpentine; magnesite formation; CO_2 sequestration, amorphous materials.

1. Introduction

Mineral carbonation is considered one of the safest and most suitable ways to sequester CO_2 (Bobicki et al., 2012; Prigiobbe et al., 2009; Sipilä et al., 2008), attempting to mimic the natural weathering of Ca/Mg-rich silicate rocks in an anthropic timescale (Gadikota et al., 2014; Kelemen and Matter, 2008). CO_2 is chemically reacted forming environmentally benign and stable carbonates. Natural Mg/Ca-bearing silicates are foreseen as potential raw materials for permanent CO_2 fixation (serpentine, olivine and pyroxenes; Dufaud et al., 2009; Gerdemann et al., 2007). Large CO_2 sequestration capacities, exceeding the total CO_2 that can be produced by burning fossil fuels (Lackner, 2003), combined with exothermically driven carbonation reactions of such

materials, enhances their potential for carbon capture and storage applications (Chizmeshya et al., 2002; Lackner et al., 1995; McKelvy et al., 2004).

Accelerating the carbonation rate relative to natural carbonation of silicate minerals is compromised by major scaling-up drawbacks (Gadikota et al., 2014; Huijgen et al., 2007; Kelemen and Matter, 2008). Pretreatment is required (heat-treatment and grinding) and aqueous slurry reactions have to be maintained at high temperatures and pressures (Benhelal et al., 2018; Farhang et al., 2016; Gerdemann et al., 2007), which stray far from post-combustion flue-gas conditions, making them currently industrially unfeasible (Linga et al., 2007).

Wet carbonation reactions of Mg-bearing minerals are proven to occur at kinetic rates feasible for CCUS applications, although they are not cost-effective (Huijgen et al., 2007). Dry gas-solid carbonation is the economically-desired reaction but, so far, this mechanism has been found inefficient (Fagerlund et al., 2012; Larachi et al., 2010; Zevenhoven et al., 2008), regardless of thermodynamically favorable exothermic reactions (Lackner et al., 1995). However, the addition of water vapor (Relative Humidity, RH: 100%) significantly enhances the kinetics of such reactions, when compared to dry gas-solid processes (Highfield et al., 2016; Loring et al., 2012), by allowing the formation of intermediate metastable hydrated magnesium carbonates (Fricker and Park, 2014; Zhao et al., 2010). The formation of these materials is kinetically favored although they are thermodynamically unstable when compared to magnesite ($MgCO_3$) (Loring et al., 2012; Schaef et al., 2013; Swanson et al., 2014). The formation of magnesite at low temperatures is inhibited by the precipitation of hydrated carbonates, possibly because of the high hydration susceptibility of Mg^{2+} ions in solution (Deelman, 2001; Felmy et al., 2012; Zou et al., 2019). The mechanisms of formation of such hydrated and anhydrous carbonates at low pressures are not well known (Hopkinson et al., 2012; Rausis et al., 2020).

Ex-situ carbonation approaches make use of available above-ground Mg/Ca-rich ores, mines tailings and wastes, which have high carbonation potential (Bobicki et al., 2012; Harrison et al., 2013; Li et al., 2018; Power et al., 2013; Sanna et al., 2012; Zarandi et al., 2017a). These alkaline industrial wastes experience milling processes that lead to a dramatic increase of their surface area and reactivity (Rigopoulos et al., 2015; Werner et al., 2013). Numerous mining sites worldwide produce or have produced easy-accessible, finely ground and highly reactive ultramafic mining wastes (Pronost et al., 2012; Thom et al., 2013; Wilson et al., 2014). Large reserves of serpentinites (also abundant among ultramafic mining wastes) are of great interest for Carbon Capture, Utilization and Storage (CCUS) applications because they may contain up to 40% MgO (Zevenhoven et al., 2008). Heat treatment of serpentine (Benhelal et al., 2019b; Bhardwaj et al., 2016; Du Breuil et al., 2019; Mouedhen et al., 2017; Pasquier et al., 2014), brucite extraction from serpentine minerals (Fagerlund et al., 2012; Highfield et al., 2016; Zevenhoven et al., 2008) or atmospheric CO_2 fixation in mine tailings (Assima et al., 2012; Power et al., 2020, 2010; Thom et al., 2013; Turvey et al., 2018; Wilson et al., 2014; Zarandi et al., 2017a) are the major mineral carbonation areas of ultramafic waste research.

Calcining serpentine minerals at temperatures between 610ºC to 790ºC dramatically enhances their carbonation reactivity (Dlugogorski and Balucan, 2014; Du Breuil et al., 2019; Farhang et al., 2017; Li et al., 2009; Mann, 2014; McKelvy et al., 2004). This process triggers the release of OH groups from the serpentine minerals, producing a highly reactive Mg-rich silicate material. The structural disorder is the main factor that controls the high-reactivity of meta-serpentine minerals towards carbonation. It has been reported that the degree of carbonation varies with residual hydroxyl water, suggesting that there is an optimal activation temperature and residence time. This can be explained by the fact that at temperatures ≤580ºC (equivalent to ≥ 45% of residual

hydroxyl water) a partial amorphization of lizardite [$Mg_3Si_2O_5(OH)_4$] by thermal dehydration occurs. However, at temperatures 720ºC and higher (equivalent to > 5 % of residual hydroxyl content) particle sintering and crystallization of Mg-rich silicate phases, such as forsterite (Mg_2SiO_4) and enstatite ($MgSiO_3$) form from the intermediate amorphous phases, reducing significantly the reactivity of such materials and therefore, should be avoided (Du Breuil et al., 2019; Li et al., 2009). These crystalline phases are not understood to directly form from serpentine minerals but rather their formation follows a topotactic transition from intermediate phases, where the formation rate of crystalline phases decreases with increasing structural disorder (Dlugogorski and Balucan, 2014). Previous research has suggested that the dehydration of lizardite occurs by lamellar nucleation and growth. Such a process may provide binding sites to new oxyhydroxide intermediate materials (McKelvy et al., 2004), such as hydrated carbonates.

Previous investigations on direct carbonation (single stage) of activated serpentine have reported a relatively low carbonation yield even under extreme temperature and pressure conditions (150 bar, 150ºC), accounting to a yield between 40-45% (Benhelal et al., 2018; Farhang et al., 2016). The mechanisms that explain such low carbonation efficiencies remain unanswered, providing further challenges in the optimization of both activation and carbonation processes (Benhelal et al., 2019b; Du Breuil et al., 2019). It has been postulated that the formation of a Si-rich passivating layer significantly contributes to this low carbonation efficiency, by limiting the diffusive effective area for Mg extraction from the core silicate phases, reducing the carbonation efficiency (Béarat et al., 2006; Daval et al., 2011; Lafay et al., 2014). More recently it was observed that such Si-rich phases could also retain a fraction of Mg (Benhelal et al., 2019b). More importantly, it was discovered that reformation of serpentine minerals may occur upon carbonation of meta-serpentines, particularly for antigorite. However, reformation of lizardite was not observed even

under extreme carbonation conditions (150 bar, 150ºC) while a limited carbonation yield was observed (~40%). Therefore, the low carbonation yields of activated lizardite are either explained by the formation of Mg-bearing Si-rich passivating phases or it remains unanswered.

Indirect carbonation routes (two stage) of activated serpentine can utilize a significantly higher Mg fraction from heat activated serpentines to form carbonate minerals than direct routes, achieving as high as 80% (Pasquier et al., 2014; Sanna et al., 2012; Werner et al., 2014). Such processes are characterized by two or more separate stages of reaction, decoupling the extraction of reactive magnesium (Mg^{2+}) form heat activated serpentine materials, followed by the reaction of the extracted Mg^{2+} with CO_2 to form carbonate minerals. This allows a better optimization of the individual steps, which not only enable a higher extraction of Mg than direct routes but also carbonate precipitation occurs typically at lower temperatures (Park and Fan, 2004; Sanna et al., 2012). Moreover, high-purity and profitable carbonates can be produced due to the removal of impurities in the steps prior to carbonation (Bobicki et al., 2012; Eloneva et al., 2012).

This work is aimed at investigating the role of partial dehydration of natural lizardite by heat activation in accelerated mineral carbonation reactions at moderately-low temperature and pressure conditions (50 - 120ºC; 6 bar) in order to provide more insights into the processes that contribute to the relatively low carbonation efficiencies during direct carbonation of activated-lizardite. Understating such processes is of paramount importance for the further optimization of both activation and carbonation processes in order to unlock the direct carbonation potential of such minerals. Lizardite was activated at different temperatures (610, 650 and 710ºC) obtaining different relative proportions of intermediate Mg-rich silicate phases. The novelty of this work is the identification of two amorphous Mg-rich silica phases upon activation, where one of these phases was observed to be highly-reactive, obtaining a complete rapid and carbonation of this

phase even under moderately-low pressures and temperatures, while the other intermediate amorphous Mg-rich phase did not carbonate, retaining a significant fraction of Mg within its disordered structure. The presence of this latter phase might provide answers to the questions raised about the low carbonation yield during direct carbonation of activated lizardite. Moreover, it was found that the distinct distribution of a highly reactive Mg-rich silicate phase among the different activated serpentines played a key role into the formation and evolution of Mg-carbonate phases, particularly regarding the formation of magnesite.

2. Materials and methods

2.1. Analytical

Crystalline phases were identified by X-Ray Powder Diffraction (XRD), using a Bruker D8™ diffractometer with Cu Kα radiation. Analyses were conducted in a 2θ deg range of 5 to 80°, with a step-size of 0.01° and measuring time of 1 second per step. Fourier Transformed Infrared Spectrograms (FTIR) were acquired by a FTIR Nicolet 6700™. An attenuated total reflection (ATR) module was used to record ATR spectra utilizing a germanium crystal (mid-IR, from 750 – 4000 cm^{-1}) of the carbonated samples. Transmission spectra of the starting materials (225-4000 cm^{-1}) were acquired for analysis of the OH vibration modes. The samples (~3% total mass) were mixed with KBr (~97%) and pressed into pellets. Data were acquired using 64 scans and 2 data point spacing. Raman spectra were obtained with an inVia Qontor™ confocal Raman microscope, equipped with a green laser with an excitation wavelength of 532 nm. Given the substantial heterogeneity of phase distribution at the microscale after reaction, Raman spectra presented below correspond to the average of 40 measurements on each sample in order to obtain representative results. Bulk chemical compositions were determined by X-ray Fluorescence Spectroscopy (XRF) by the fusion bead method on a UniQuant® apparatus from Thermo Fisher Scientific™.

Temperature Programmed Desorption of CO_2 and H_2O (CO_2, H_2O-TPD) analysis was acquired by BELCAT-M™ instrument equipped with Thermal Conductivity Detector (TCD) in order to measure the amount of CO_2 stored in the reacted samples. Data were acquired at a heating rate of 10ºC/min from room temperature to 850ºC, under a He flow of 50mL/min. Calibration of the CO_2 signal of the TCD was carried out on the basis on measuring the moles of CO_2 from different known gas mixture compositions varying the CO_2/He proportions (0.34; 0.18; 0.10). Calibration of the water vapor signal was carried out by measuring the moles of water vapor originated from calcining (using a heating rate of 10ºC/min) brucite (>99% BioUltra CAS number: 1309-42-8), $Mg(OH)_2$. Secondary-electron Scanning Electron Microscopy (SEM) imaging of powder samples was carried out with a cross-beam work station Zeiss Neon 40™ workstation, operated at 5keV. The particle size distribution of samples was measured by a Malvern Panalytical MasterSizer 3000. Analysis were performed in an aqueous dispersion of the solid samples in deionized water. In this study, an uncertainty of ±5 % in the particle size analysis was considered.

2.2. Samples

Serpentines were obtained from the Hispaniola Island, located in an orogenic complex at the northern edge of the Caribbean plate. Powder XRD analysis confirmed that the starting material was composed of lizardite (Figure S1a). Other serpentine phases (e.g. antigorite, chrysotile) were not observed. Minor magnetite ($Fe^{3+}_2\ Fe^{2+}\ O_4$) was also identified (serpentinites generally contains from 5 to 15 magnetite wt%.). The oxide composition of the material was determined by XRF: SiO_2, 41.45; TiO_2, 0.01; Al_2O_3, 0.59; Fe_2O_3, 8.71; MnO, 0.11; MgO, 35.98; CaO, 0.10. Loss of ignition accounted for 12.24 wt.% of the original material which is slightly lower than the water content from stoichiometric lizardite (13.04 wt%.). The atomic Mg/(Mg+Fe) ratio was 0.805.

Detailed information of the sample's geochemistry can be found in Marchesi, et al., 2016 (Marchesi et al., 2016).

2.3. Experimental procedure

The material was subjected to a prograde heating rate of 1ºC/min up to 610 (AS610), 650 (AS650) and 710ºC (AS710) respectively, and maintained for 16h at the desired temperature, generating an activated Mg-rich silicate material (product of the amorphization of lizardite; Figure 1, S1). Prior to heat treatment, the material was ground to a powder and sieved to obtain grains of size smaller than 45 µm (Figure S1b). A detailed analysis of the starting material and the evolution of Mg-rich silicate phases upon activation can be found in section S1 and S2, respectively.

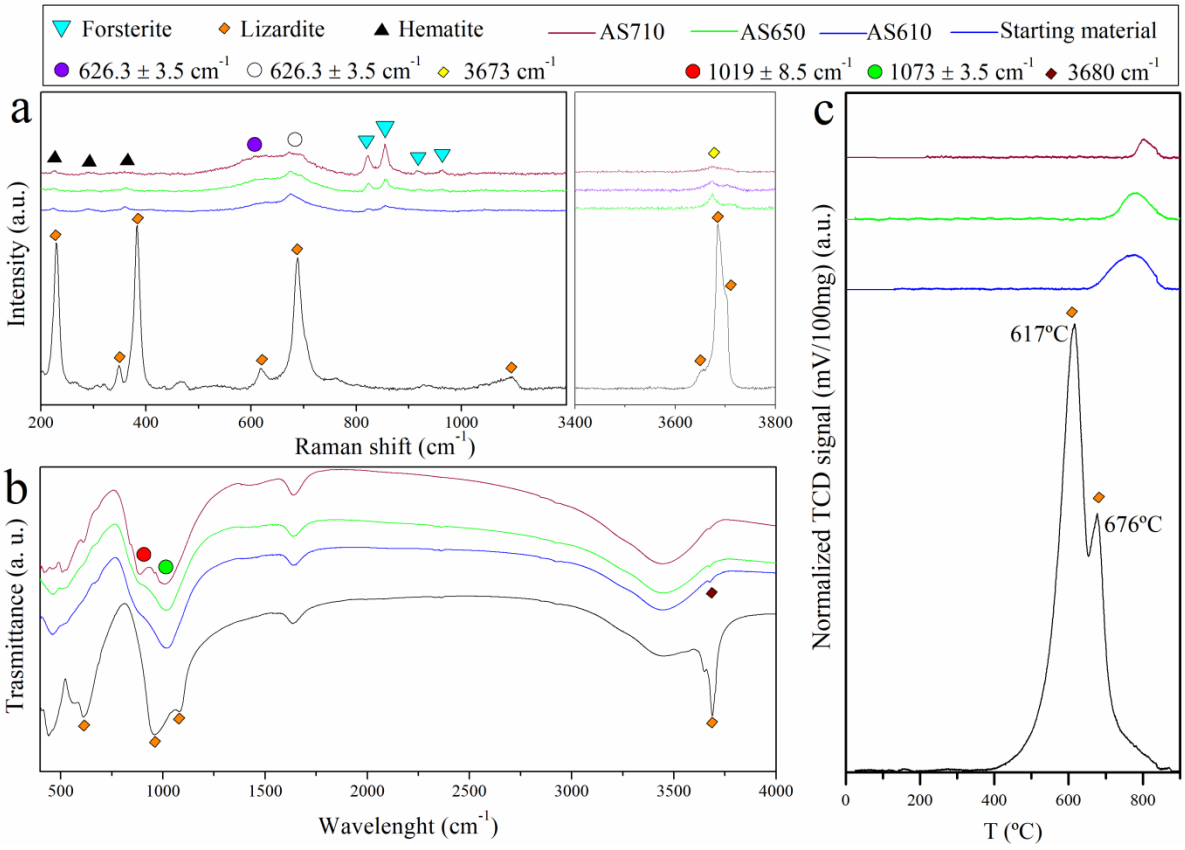

Figure 1. (a) Raman, emphasizing the OH vibration region, (b) FTIR, (c) TPD analysis of the starting materials and the products after heat activation

The direct moist carbonation experimental setup consists of a stainless steel pressurized continuous flow reactor placed within a furnace with an integrated thermocouple (Scheme S1; Rausis et al., 2020). Heat activated lizardite was loaded into the reactor and heated to the desired temperature (50, 90 and 120ºC), using N_2 as a carrier gas (in order to avoid reaction of the activated materials with CO_2 during heating or cooling). Then, CO_2 was introduced into the system and the pressure was adjusted by pressure regulators and a back-pressure regulator, achieving a constant value of 6 bar for a given gas flowrate. Prior to introduction in the reactor, CO_2 flowed through a ~50 mL vessel containing water; temperature and pressure were chosen to produce an estimated gas mixture with > 90% RH. Conditions were kept isothermal during different reaction times, from 30 minutes to 4 hours. After the experiments, pressure was released and N_2 was used to purge the residual CO_2 while cooling. CO_2 and water vapor partial pressures were estimated by the saturated water vapor pressure Antoine equation and Raoult's law. CO_2 partial pressure accounts for 5.9, 5.4 and 4.2 bar for 50, 90 and 120ºC experiments, respectively. Water vapor partial pressure accounts for 0.1, 0.6 and 1.8 bar for 50, 90 and 120ºC experiments, respectively. Table 1 summarizes the experiments carried out as well as the specific partial pressures for both CO_2 and $H_2O_{(g)}$ of each experiment.

Activated material	**Time (h)**	**50ºC**	**90ºC**	**120ºC**
		P_{CO2}: 5.9; $P_{H2O(g)}$: 0.1	P_{CO2}: 5.4; $P_{H2O(g)}$: 0.6	P_{CO2}: 4.2; $P_{H2O(g)}$: 1.8
AS610	0.5	Nsq	Dyp, AMC	Hmg
	1	Nsq	Dyp	Hmg
	2	Nsq	Dyp	Hmg, Mag

	4	Nsq	Dyp	Hmg, Mag
AS650	0.5	Nsq	Dyp, AMC	Hmg
	1	Nsq	Dyp	Hmg
	2	Nsq	Dyp	Hmg
	4	Dyp, AMC	Dyp	Hmg, Mag
AS710	0.5	Nsq	Dyp, AMC	Hmg
	1	Nsq	Dyp, AMC	Hmg
	2	Nsq	Dyp	Hmg
	4	Dyp, AMC	Dyp	Hmg, Mag

Table 1. Summary of the carried experiments, specific experimental conditions and the identified carbonate phases. P_{CO2} and $P_{H2O(g)}$ stands for CO_2 and H_2O vapor partial pressure, respectively. CO_2 dilution with water vapor (relative humidity ≥ 90%) was estimated following the saturated water vapor pressure Antoine equation and Raoult's law. Nsq: Nesquehonite, Dyp: Dypingite, Hmg: Hydromagnesite, Mag: Magnesite, AMC: possibly an amorphous Mg carbonate.

3. Results and discussion

3.1. Formation of Mg-carbonate phases

Newly formed carbonates were identified upon reaction of the three different activated lizardites. Figure 2 shows the Raman spectra of the reaction products from experiments carried at 50, 90 and 120ºC during 30 minutes to 4 hours at 6 bar. At 120ºC two newly formed peaks were identified (1094.2 ± 0.4, 1116.6 ± 0.3 cm^{-1}) within the region of the characteristic of the ν_1 symmetric stretching mode (ν_{1sym}) of the carbonate ion (CO_3^{2-}) (Edwards et al., 2005; Frost, 2011) for all three

activated materials. The 1094.2 ± 0.4 peak is correlated to the emergence of the 324.9 ± 0.5 peak in the lattice vibration region (100-500 cm^{-1}). Such peaks are especially evident in AS610, and they are only observed at 2 and 4 hours. Those peaks might suggest the presence of magnesite ($MgCO_3$).

Comparison between the Full Width Half Maximum (FWHM) and peak position of the ν_{1sym} carbonate peak of the reaction products is shown on Figure S3. Calculated data from experiments carried out at 120ºC show that the 1094.2 ± 0.4 cm^{-1} peak fit well with reference magnesite for all the pretreated materials. For AS610 materials, the second peak (1116.6 ± 0.3 cm^{-1}) fits very well with hydromagnesite, $Mg_5(CO_3)_4(OH)_2 \cdot 4(H_2O)$. However, for AS650 and AS710, this peak is approaching the reference data for dypingite, $Mg_5(CO_3)_4(OH)_2 \cdot 5H_2O$. This latter mineral has a similar composition to hydromagnesite but it is structurally more disordered with a variable amount of water molecules per unit (Canterford et al., 1984; Davies and Bubela, 1973; Rausis et al., 2020).

Two different peaks ν_{1sym} were identified after reactions performed at 90ºC (1093.4, 1118.9 ± 1 cm^{-1}). The position of both peaks remains constant for all the activated materials, irrespective of their reaction times. The first peak (1093.4 cm^{-1}) despite having similar position to that of magnesite, does not emerge together with the lattice vibration peak of magnesite (324.9 ± 0.5), suggesting the presence of a different carbonate phase. Calculated FWHM vs peak position shows that the 1093.4 cm^{-1} peak does not correlate with any other represented Mg-carbonate phase (Figure S3). Such peak is similar to the one observed by previous studies (Rausis et al., 2020), which suggest that this peak might be associated with a hydrous amorphous Mg-carbonate (AMC) phase that has similar composition and dehydration temperature ranges to nesquehonite. This peak is only observed at 30 minutes of reaction for AS610 and AS650. However, this peak is not

observed until 1 hour of reaction for the AS710 experiments. The inexistence of this peak at longer reaction times (2 and 4 hours) suggest that the phase responsible for this peak acts as precursor to the phase associated with the 1118.9 ± 1 cm^{-1} peak.

The second peak (1118.9 ± 1 cm^{-1}) appears to be slightly shifted when compared to the one observed from 120ºC experiments (1116.6 ± 0.3 cm^{-1}). The calculated FWHM vs peak position data shows a good fit with reference dypingite.

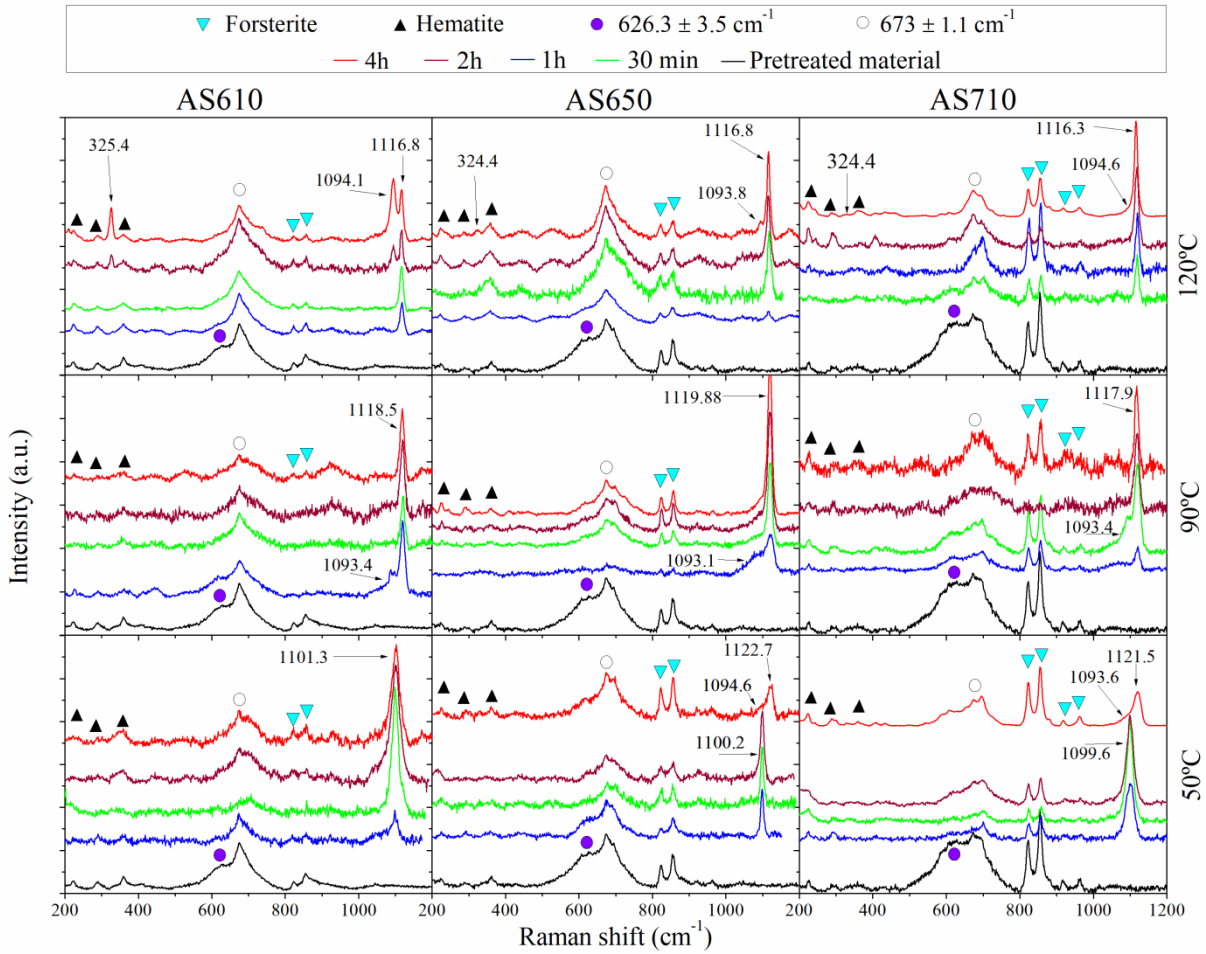

Figure. 2. Raman spectra of three different meta-serpentine (activated at 610, 650 and 710ºC) and the reaction solid products from experiments carried at 50, 90 and 120ºC from 30 minutes to 4 hours.

Analyses of the solid products from experiments performed at 50ºC show the presence of three different peaks (1094.1 ± 0.5, 1100.5 ± 0.9, 1122.1 ± 0.6 cm^{-1}) within the ν_{1sym} region. At this temperature, clear differences are observed for different activated materials. The 1094.1 ± 0.5 cm^{-1} peak is similar to the one observed at 90ºC (associated with a possible AMC). The second peak (1100.5 ± 0.9) fits well with reference nesquehonite, $Mg(HCO_3)(OH)\cdot 2(H_2O)$, only for the AS650 materials. For AS610 and AS710, such peak is observed to be in similar position as nesquehonite but wider. Moreover, AS610 materials shows the presence of only the 1100.5 ± 0.9 peak at any reaction time. This peak is only identified from 30 minutes to 2 hours of reaction for the AS650 and AS710 materials. However, at 4 hours, it is no longer identified and two distinct peaks have emerged (1094.1 ± 0.5 and 1122.1 ± 0.6 cm^{-1}). This suggests that the 1100.5 ± 0.9 peak nourishes the growth of these two latter peaks, in agreement with recent studies (Rausis et al., 2020). The 1122.1 ± 0.6 cm^{-1} peak is only observed for AS650 and AS710 and has the similar position with reference dypingite but with higher FWHM, probably suggesting a highly disordered structure (Rausis et al., 2020). The emerged 1094.1 ± 0.5 cm^{-1} peak is associated with a possibly amorphous phase, as previously discussed. FTIR analysis also evidences the formation of carbonates, and the observed phases are consistent with Raman observations (Figure 3; see section S3)

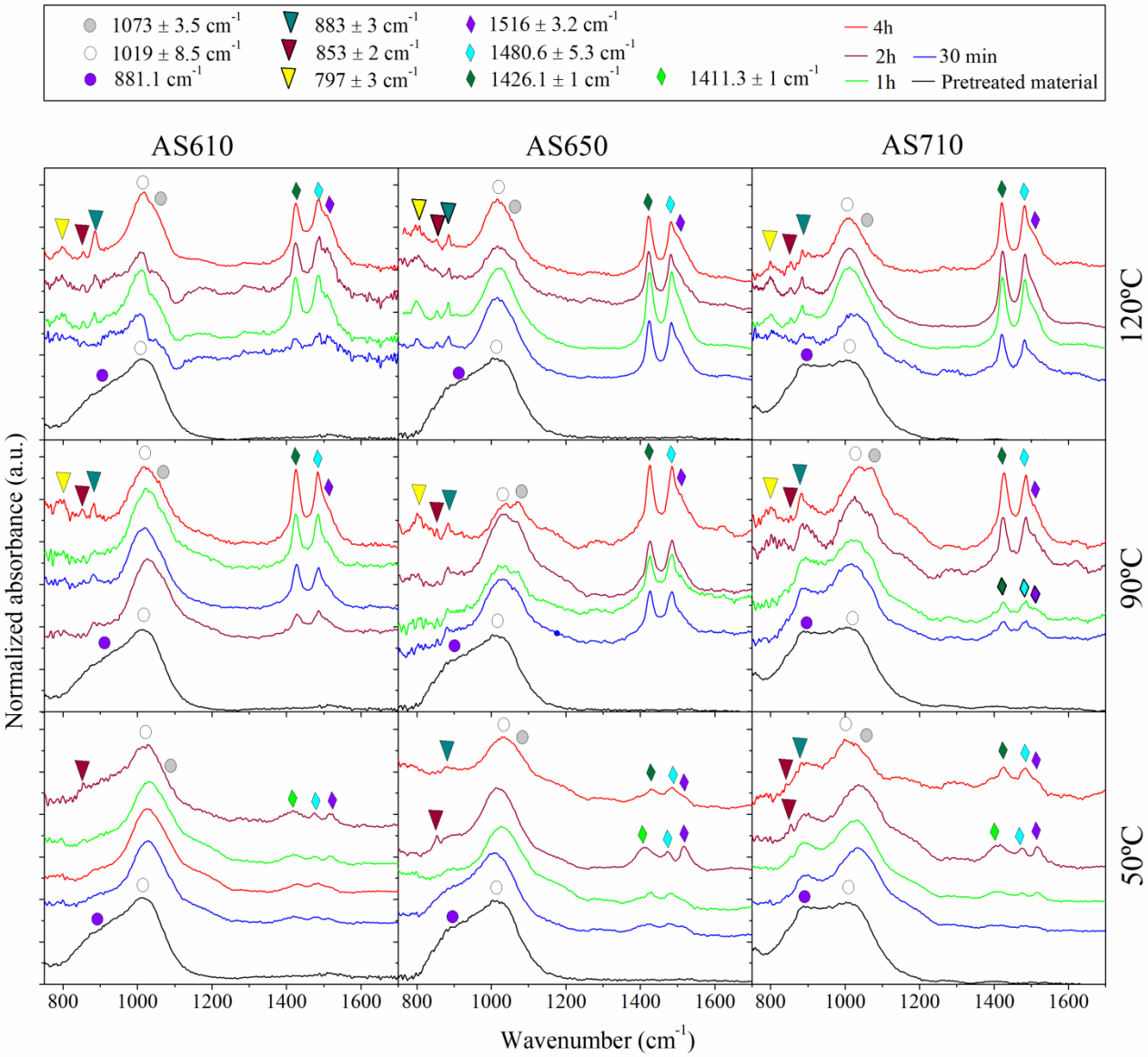

Figure 3. FTIR-ATR analysis of the pretreated and carbonated materials at 50, 90 and 120ºC and 6 bar, from 30 minutes to 4 hours.

XRD analysis of the activated and carbonated materials (Figure 4) corroborates Raman and FTIR observations. At 120ºC, characteristic XRD patterns for hydromagnesite (Fricker and Park, 2013; Schaef et al., 2013) were identified for all the activated materials, and magnesite (Giammar et al., 2005; Schaef et al., 2013) only for the AS610 and AS650 materials. A hydromagnesite-dypingite

phase was observed at 90ºC, resembling XRD features observed by Hövelmann et al., 2012. Nesquehonite was observed only at 50ºC for AS610. On the other hand, AS650 and AS710 shows the presence of a highly disordered dypingite-like phase. The identification of different carbonate phases for different activated material under identical carbonation conditions suggest that the activated materials play a key role not only in the formation of carbonate phases but also in their evolution during carbonation reactions.

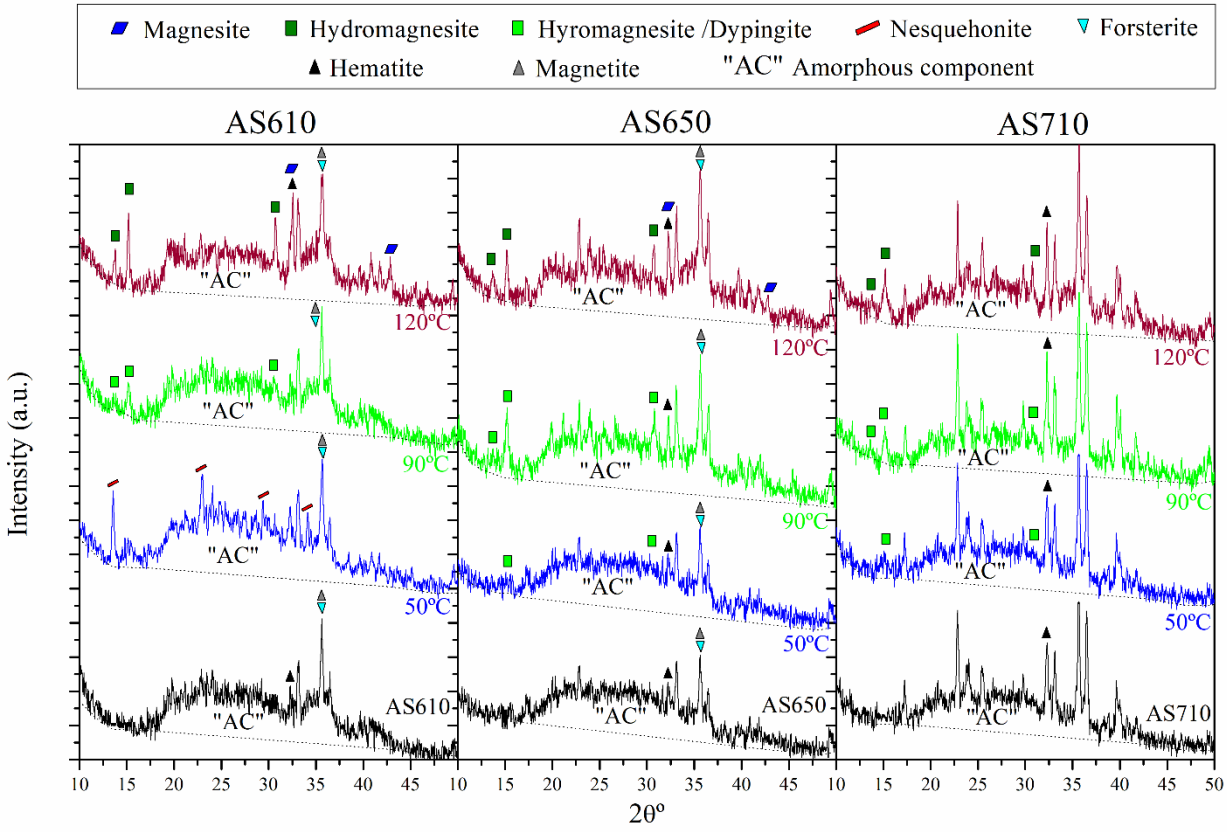

Figure 4. XRD analysis of the activated and carbonated materials at 50, 90 and 120ºC during 4 hours. Unmarked peaks also correspond to forsterite.

Evolution of the carbonation reaction was also monitored by SEM (Figure 5). Hydromagnesite plates, arranged in rosettes of crystals ≥1µm in size (as in Maroto-Valer et al., 2005 and Power et al., 2019) are observed in the AS610 materials carbonated during 1h at 120ºC (Figure 5a) as well

as a progressive formation to euhedral magnesite (~1µm) (Prigiobbe and Mazzotti, 2013) over time (2h, Figure. 5b; 4h, Figure 5c). Figure 5b inset and c shows that an aggregation of hydromagnesite and magnesite crystals respectively, which were possibly formed by nucleation and crystal growth (Giammar et al., 2005).

Elongated and prismatic rod-like structures (~5µm), with morphological features resembling those of nesquehonite (Hänchen et al., 2008; Zarandi et al., 2017b), were identified in the 30 minutes experiments at 90ºC for AS610 materials (Figure 5d). On this prismatic structure is observed overgrowths of flaky nanocrystals (<100nm) and more developed flaky microcrystals (<1µm), exhibiting features of the "house of cards" texture, which is characteristic of the transformation of nesquehonite to hydromagnesite or dypingite (Hao and Du, 2009; Hopkinson et al., 2012; Power et al., 2016; Rausis et al., 2020). The smaller, nanometer-sized crystals also form sub-spherical aggregates, similar to those reported by Zarandi et al., 2017. Only a dypingite-like phase, possibly coexisting with an amorphous phase (Rausis et al., 2020), were identified with Raman and XRD. Therefore, the rod-like structure might be evidence that the identified dypingite might have formed from the transformation of an early-nesquehonite, exhibiting a well-developed "house of cards texture". Such transformation mechanism is a good example of the Ostwald step rule (Morse and Casey, 1988). This texture is commonly observed on dissolution-recrystallization self-assembly growth mechanisms. Therefore, this may imply a possible surface water layer mediating the dissolving-recrystallization mechanism (Taifan et al., 2016). This layer may stem from either molecular water of the dissolving mineral or from the condensation of water vapor.

After 1 hour of reaction, experiments performed at 90ºC for AS610 showed only rosette crystal arrangements made of dypingite flakes were observed (Figure 5d), resembling features observed by Hopkinson et al., 2008.

Experiments performed at 50ºC and 2h for AS650 produced massive rod crystals characteristic of nesquehonite (Figure 5f). However, analogous experiments on AS710 showed acicular aggregates that are texturally comparable to nesquehonite (Hopkinson et al., 2008) (Figure 5g). Raman and XRD analysis showed that the massive nesquehonite has similar FHWM peak to the reference mineral. However, broader peaks with the same peak position as reference nesquehonite are associated to the acicular aggregation of oriented prismatic crystals. Carbonation of the AS710 material during 4h results in the formation of rosette crystal arrangements conforming to dypingite morphology (Figure 5h), indicating the transformation of nesquehonite to dypingite, as also suggested by the Raman and XRD results.

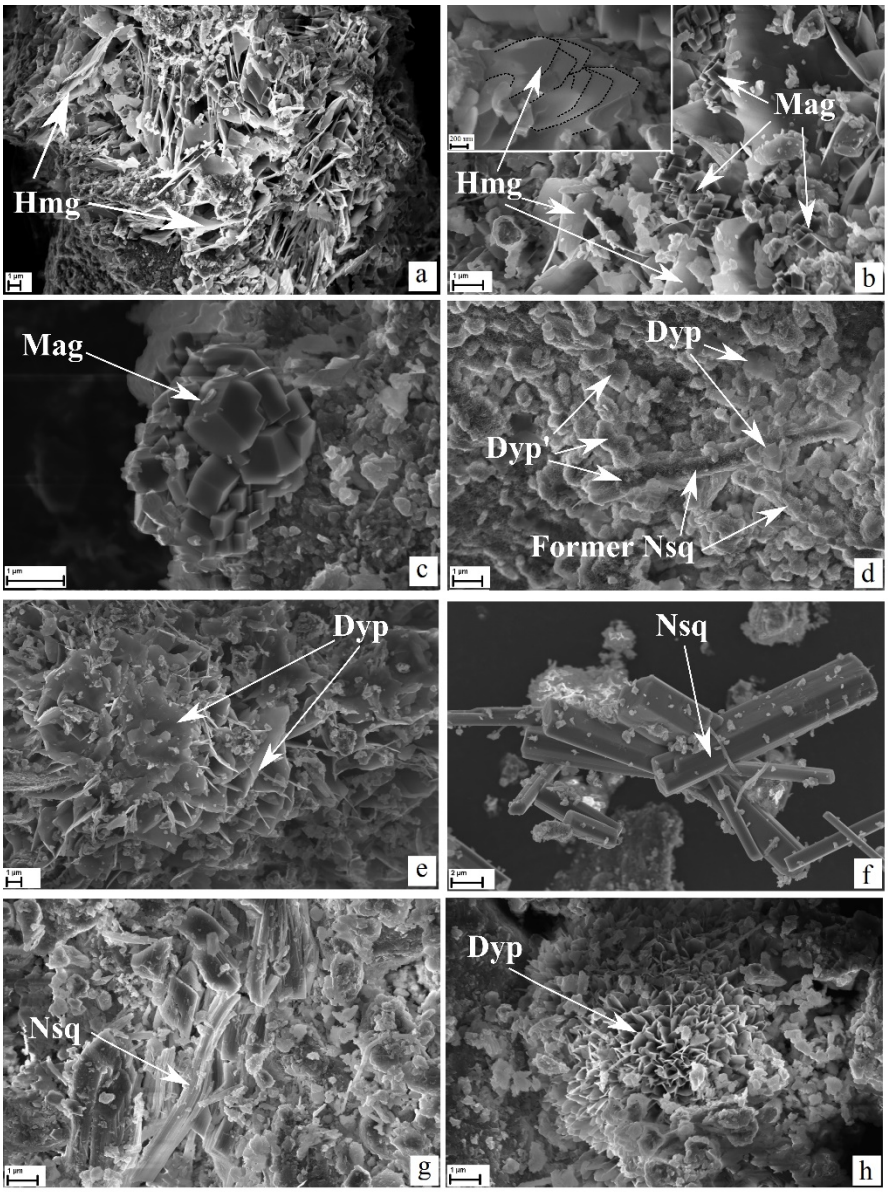

319

320 **Figure 5.** Representative SEM images of carbonated samples. AS610 carbonated at 120ºC for 1h
321 (a), 2h (b) and 4h (c); at 90ºC for 30min (d) and 1h (e). Reaction products of AS650 obtained at
322 50ºC after 4h (f). Carbonated products of the AS710 materials carbonated at 50ºC for 2h (g) and
323 4h (h). Hmg: hydromagnesite, Mag: magnesite, Dyp': nano-dypingite (<100nm), Dyp: dypingite,
324 Nsq: nesquehonite.

The estimated CO_2:H_2O ratios of the carbonate products (calculated from TPD data; see section S4, S5) are consistent with the stoichiometric composition of the identified carbonates as summarized in table 1.

3.2. Evolution of Mg-rich silicate phases upon carbonation

The intensity of the wide Raman peak located at 626.3 ± 3.5 cm^{-1} (which emerged from thermal activation, Figure 1a) is diminishing as the carbonation reaction proceeds, probably suggesting that the phase (responsible for this Raman broad peak) partially or fully nourishes the formation of carbonates (Figure 2). Since forsterite and minor hematite/magnetite were the only identified crystalline phases upon activation (as Q_3 dehydroxylate II was not identified), the presence of the Raman broad peak located at 626.3 ± 3.5 cm^{-1} might be associated with an amorphous Mg-rich silicate phase, product of the amorphization of lizardite. However, the 673 ± 1.1 cm^{-1} peak (which also might be associated with an amorphous Mg-rich silicate phase) remained relatively unchanged upon carbonation. Therefore, this might suggest that these two Raman peaks are associated with two different amorphous Mg-rich silicate phases (possibly to Q_1 dehydroxylate I and "Q_2 amorphous enstatite", since such phases are the only known amorphous intermediate phases of activated lizardite, see section S2), with the phase responsible for the 626.3 ± 3.5 cm-1 Raman peak, being the most reactive. To our knowledge, this is the first evidence of the significantly different reactivity of two coexisting intermediate amorphous Mg-rich silicate phases that form upon activation.

FTIR analyses show changes to the Si-O-Si stretching modes region are observed after carbonation (Figure 3). Upon carbonation, two peaks are observed (1019 ± 8.5 and 1073.55 ± 3.95

348 cm^{-1}). The 1019 ± 8.5 cm^{-1} peak (as also observed in the activated materials) remains relatively
349 unchanged, possibly indicating that the intermediate phase responsible for this peak as well as
350 overlapping forsterite remained seemingly unreacted upon carbonation. On the other hand, the
351 888.1 cm^{-1} broad peak (observed in the activated materials) is no longer identified upon
352 carbonation and an emerging well-defined peak at similar position is observed (883 ± 3 cm^{-1}),
353 characteristic of hydromagnesite-like phases and magnesite. The intermediate phase responsible
354 for the 888.1 cm^{-1} broad peak was the only identified reactant upon carbonation, indicating that
355 this phase is partially or fully nourishing the formation of carbonates. Comparison with Raman
356 results (Figure 2) and the analysis of the starting materials (Figure 1, S1) suggest that the phase
357 responsible for the 888.1 cm^{-1} FTIR broad peak might be associated with a highly reactive
358 amorphous Mg-rich silicate phase (HRAS), which is strongly associated with the phase responsible
359 for the 626.3 ± 3.5 cm^{-1} Raman peak. Analogously, the unreacted 1019 ± 8.5 cm^{-1} FTIR peak might
360 also be associated with the poorly-reactive amorphous phase (PRAS) responsible for the 673 ± 1.1
361 cm^{-1} Raman peak.

362 Moreover, the 888.1 cm^{-1} FTIR band associated with the reactive amorphous phase observed
363 during this study might also not contain a silanol group (Benhelal et al., 2019b), as this functional
364 group (as well as siloxane and Si-O-Al^{2+}/Na^{2+}/Mg^{2+} groups) is associated with the formation of a
365 Si-rich passivating layer (Casey et al., 1988; Chizmeshya et al., 2006; Hellmann et al., 1990; Lafay
366 et al., 2014), since it is inconsistent with the highly-reactive nature of this intermediate and
367 probably amorphous Mg-rich silicate phase.

368 The identified peak at 1073.55 ± 3.95 cm^{-1} (formed upon carbonation and different from the un-
369 activated lizardite, Figure 1b) might suggest the formation of phases containing siloxane groups
370 (Benhelal et al., 2019b) or amorphous silica (Tran et al., 2013). This is consistent with the

formation of a passivating Si-rich phase (Chizmeshya et al., 2006; Hellmann et al., 1990; Lafay et al., 2014), Numerous studies have reported that such phases play an important role in the passivation of the carbonation reaction (Béarat et al., 2006; Julcour et al., 2015). A fraction of Mg can also be stored in this Si-rich phase reducing the available Mg fraction to form carbonates (Benhelal et al., 2019b).

XRD studies also show the presence of a broad hump from 17 to 43 2θº in all the analyzed samples, suggesting the presence of an amorphous component (Blue et al., 2017; Fukushi et al., 2017; McKelvy et al., 2004) even after carbonation (Figure 4), maybe accounting for the unreacted PRAS, Si-rich passivating phases and, in some experiments, amorphous carbonates mentioned above.

In a recent study it was observed that the recrystallization of serpentine minerals from the intermediate phases may occur upon direct aqueous carbonation at elevated pressures (120-150 bar) of activated serpentine, particularly for antigorite (Benhelal et al., 2019b). As discussed by the authors, the re-crystallization of serpentine is considered to be an un-desired reaction, as such reaction increases the energy penalty of the overall reaction and competes with carbonation (consuming a fraction of the available reactive Mg from amorphous intermediate phases) reducing the reaction efficiency. In this study, the re-formation of lizardite upon carbonation of the activated materials was not observed as evidenced by the lack of its characteristic Raman, XRD, FTIR and TPD features upon carbonation.

The reactivity towards mineral carbonation of activated serpentine is primarily due to its amorphous nature (Dlugogorski and Balucan, 2014; Mann, 2014; McKelvy et al., 2004). Du Breuil et al., 2019a quantified the intermediate phases that formed during activation of lizardite at different temperatures and reported that such values have a linear correlation with the obtained

carbonation efficiency upon reaction with CO_2. In this study, the coexistence of HRAS and PRAS played a crucial role in the moist carbonation reactions, since it was consistently observed that the HRAS was the main or only phase that contributed to the formation of carbonates. On the other hand, PRAS remained unreacted upon carbonation. This observation provides important and novel insights for direct carbonation processes of activated serpentine. The formation of HRAS upon activation is desired since it is highly reactive even under moderately low pressures (6 bar; 120ºC). Such pressure and temperature conditions are close to industrial flue gas emissions (Highfield et al., 2016; Rausis et al., 2020; Swanson et al., 2014). This strongly suggests that high pressures and temperatures are not required for the carbonation of this phase. On the other hand, PRAS can be considered as un undesired product of activation, since it is significantly less reactive than HRAS and also fixes a significant amount of Mg within its disordered silicate structure.

In this study, no evidence of forsterite carbonation was observed. This is consistent with previous observations where intermediate amorphous silicate phases (formed upon serpentine heat activation) are more reactive than forsterite. However, it has been reported that the carbonation of forsterite is partially unlocked at high pressures and temperatures (185ºC and 150 bar) achieving even higher reactivity than for activated lizardite (Gerdemann et al., 2007).

3.3. Time resolved carbonation efficiency

The extent of carbonation (expressed as g CO_2 /100 g of sample), as well as the estimated Mg fraction fixed by carbonates based on TPD data (Figure S4, S5; see section S6) are shown in Figure 6. Higher temperature pretreatments induced a lower carbonation yield. A maximum of 9.3g of CO_2 sequestered per 100 grams of sample was achieved at 120ºC and 4h for AS610, which accounts to 23.3% of the available Mg fraction fixed by carbonates.

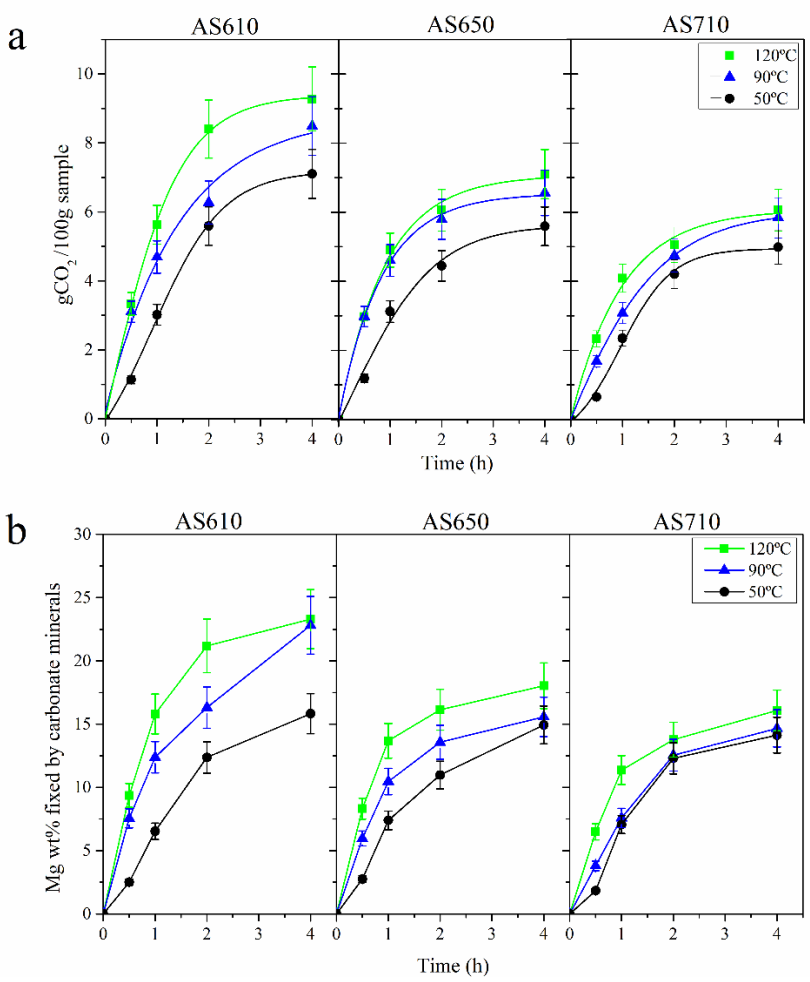

Figure 6. (a) Grams of CO_2 sequestered per 100 grams of sample, as estimated from TPD analysis. **(b)** Amount of Mg fixed by carbonate minerals after carbonation of AS610, AS650 and AS710. Error bars take into account the phase variability and the calculated data from three analogous experiments.

The limited extraction of Mg from intermediate silicate phases upon carbonation implies that the reaction has been partially inhibited during the studied timeframe. The coupled formation of carbonates and amorphous silica plays an important role in the passivation of the reaction, as previous studies have reported (Béarat et al., 2006; Benhelal et al., 2019a; Julcour et al., 2015).

The presence of magnetite and hematite may play a role in the passivation of the carbonation reactions, as previous work has discussed (Fauth et al., 2002; Mouedhen et al., 2017).

The lower carbonation yield observed for AS650 and AS710 relative to AS610 is probably due to undesired nucleation of forsterite from intermediate phases upon thermal activation, as has been extensively reported in previous studies (Dlugogorski and Balucan, 2014; Du Breuil et al., 2019; McKelvy et al., 2004). Moreover, the larger particle sizes of materials activated at 650 and 710ºC and hence, lower overall surface area, probably contribute to their lower carbonation yield (Figure S1b). However, it has been reported that the reactivity of activated lizardite is likely to be more influenced by the mineralogy than by surface area (Du Breuil et al., 2019). In the context of this paper, the Mg fraction from AS710 that forms carbonates is only up to 7% lower than in the case of AS610, despite the significant higher yield of forsterite in the materials activated at 710ºC. This might indicate that the nucleation of forsterite, despite reducing the carbonation yield, is not the main reason for the reduced carbonation yield of activated lizardite. On the other hand, undesired re-crystallization of lizardite was not observed upon carbonation. Therefore, the main limiting factor of the direct carbonation of activated lizardite is either attributed to the formation of passivating phases or there are limiting factors that are yet undefined.

Only one highly-reactive phase (HRAS) is formed upon thermal activation of lizardite (see section 3.2). The formation of both intermediate PRAS (this study) and Q^3 dehydroxylate II (Farhang et al., 2016) are undesired due to their low reactivity and they fix a significant fraction of available Mg. Moreover, the carbonation of HRAS results in the formation of carbonates as well as a Si-rich phase formed that might retained a fraction of Mg, which further limits the extent of reaction, aside from its characteristic passivating nature. These limiting factors, particularly the formation of PRAS, might be responsible for the yet unanswered limited carbonation efficiencies

obtained via direct aqueous and moist carbonation of lizardite. It may also provide important insights in the optimization of both activation and carbonation processes of activated lizardite. These limiting factors are considered to reduce the carbonation yield significantly more than the nucleation of forsterite in AS710 relative to AS610.

Bhardwaj et al., 2016 reported a rapid and limited direct moist carbonation of activated lizardite at low pressures and temperatures (1 bar, 65-95ºC), sequestering a maximum of 7.5g of CO_2 per 100g of sample. Similar results were also reported by Veetil et al., 2015 (7gCO_2/100g sample) upon direct moist carbonation of activated lizardite, although at significantly higher temperature and pressure (200ºC, 25bar). Such limited carbonation efficiencies are slightly lower than those obtained in this work. The reduced carbonation yields obtained in this study and those reported by Bhardwaj et al., 2016 and Veetil et al., 2015 are likely attributed to the limited abundance of HRAS in these activated serpentines.

On the basis of these observations, activation processes for lizardite can be further optimized by adjusting activation temperature and residence time in order to (i) obtain a complete or almost complete transformation of lizardite as well as a complete transformation of Q^3 dehydroxylate II to amorphous intermediate Mg-rich silicate phases, (ii) increase the proportion of HRAS relative to PRAS (this study) and (iii) avoid the nucleation of forsterite and enstatite as well as particle sintering. This might be achieved by heat activating lizardite at 750ºC for 15 min (Du Breuil et al., 2019) or at lower temperatures over prolonged residence times (610ºC for ≤16h; this study). Carbonation and activation processes should be focused on minimizing the passivation effect due to undesired reactions and the formation of passivating layers (if possible). Moreover, the direct carbonation conditions at which these materials are tested could be significantly optimized by working at moderately low pressures (≤10 bar; see section S7).

3.3.1. Magnesite formation

The Mg wt% stored by hydromagnesite and magnesite was possible to estimate since the associated thermal decarbonation associated with those minerals (observed with TPD, Figure S4) were differentiated (Figure 7). Hydromagnesite formation reached a steady state at 1h for AS610 and at 2h for AS650 and AS710, accounting to ~15% of the total available Mg in activated materials. This possibly indicates that some process is hindering the formation hydromagnesite, even if sufficient Mg^{2+}, CO_2 and H_2O are available. One possibility is that the reaction environment is saturated with respect to hydromagnesite. Magnesite only started forming once hydromagnesite formation had reached the steady state.

The formation of magnesite from direct aqueous carbonation requires relatively high temperatures (>100ºC), elevated CO_2 partial pressures (~100 bar) and/or extended reaction times (Hänchen et al., 2008; Hopkinson et al., 2012; Montes-Hernandez et al., 2012; Swanson et al., 2014). In this study, magnesite was observed to form at 2h of reaction at moderately low pressures and temperatures (120ºC, 6bar) upon AS610 direct moist carbonation. Our results suggest that the formation of magnesite is greatly accelerated once the formation of hydromagnesite reached a steady state and sufficient Mg^{2+} is available. Magnesite content was estimated to be lower for the higher temperature activated materials. This might be explained by the slower formation of hydromagnesite on such materials, delaying the time needed for hydromagnesite formation to reach the steady state.

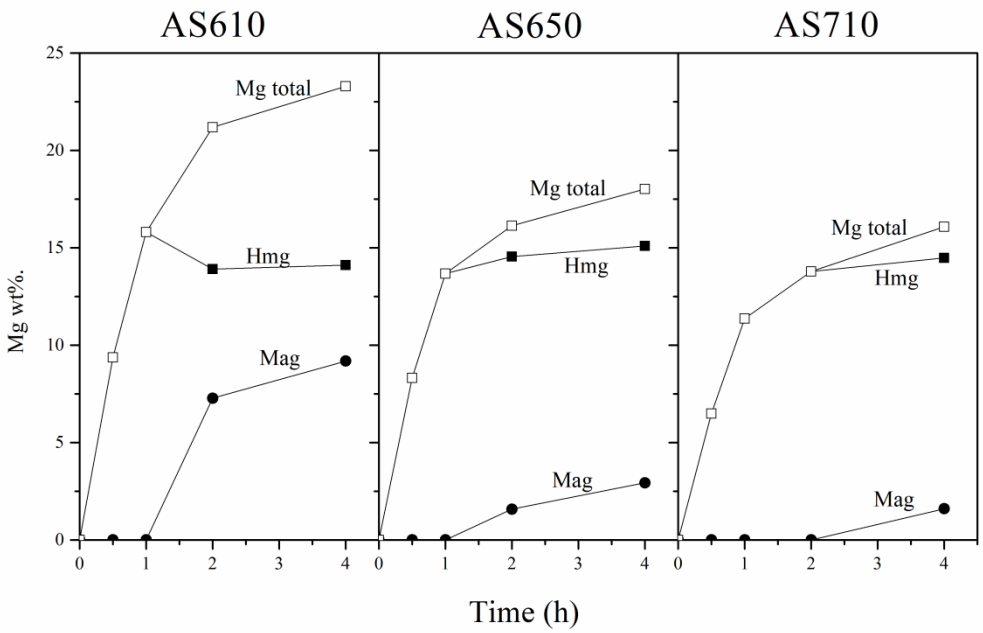

Figure 7. Mg wt% stored in carbonate minerals after carbonation of AS610, AS650 and AS710 at 120ºC, from 30 minutes to 4 hours. (Mg total) Mg wt%. that has been stored by both (Hmg) hydromagnesite and (Mg) magnesite.

The formation of different carbonate phases under analogous experimental conditions among the different activated-serpentines, suggest that the different relative proportion of HRAS relative to PRAS among such materials plays a key role on the formation and evolution of Mg-carbonate phases, as observed for the accelerated formation of magnesite as well as transition of nesquehonite to dypingite-like phases and possibly to a hydrous AMC.

4. Conclusions

This experimental study provides new insights on both the role that the intermediate phases of three different meta-lizardites (pretreated at 610, 650 and 710ºC) play during carbonation and the formation of hydrated and anhydrous Mg-carbonates. The reaction temperature is the dominant factor that controls the formation of the different carbonate phases and their hydration level. At

120ºC, hydromagnesite and magnesite were identified. Magnesite only appeared when hydromagnesite formation reach a steady state, especially for the 610ºC activated materials. This may suggest that magnesite formation might be accelerated once hydromagnesite formation reached an steady state and sufficient Mg^{2+} is available. At 90ºC, probably nesquehonite (formed in less than 30 minutes) transformed into the identified dypingite-like phases and probably an amorphous carbonate phase. Nesquehonite remained untransformed from experiments performed at 50ºC only for the 610ºC activated materials. However, for the higher temperature activated materials (650 and 710ºC), it was completely transformed (from 2 to 4 hours of reaction) into a highly-disordered dypingite and probably an amorphous carbonate phase.

Different carbonate phases were identified during analogous carbonation experiments between the three different activated materials, suggesting that the reacting materials play a key role in carbonate phase formation and evolution. This might be attributable to the possible coexistence of different amorphous Mg-rich silicate phases that were formed upon lizardite activation and the distribution of such phases depending on the activation temperature. It was found that two different amorphous Mg-rich silicate phases were formed upon activation. The amorphous phase associated with the 888.1 and 626.3 ± 3.5 cm^{-1} FTIR and Raman peak, respectively, is found to be highly-reactive, as this phase exclusively or mainly nourished the formation of carbonates. A complete carbonation of this phase could be obtained at moderately-low pressure and temperature conditions with reasonable conversion rates. The other amorphous phase, associated with the 673 ± 1.1 and 1019 ± 8.5 cm^{-1} FTIR and Raman peak, respectively, remains seemingly unreacted upon carbonation. The presence of this poorly-reactive phase might provide important insights to the yet unanswered question regarding the limited carbonation yield during direct carbonation of activated serpentine routes, since, upon activation and carbonation, it retains a significant fraction

of Mg within its disordered structure. Moreover, forsterite nucleation in the materials activated at 710ºC yielded only up to 7% decrease on the extracted Mg fraction to form carbonates when compared to the materials activated at 610ºC. This strongly suggests that the nucleation of forsterite, despite reducing the carbonation yield, is not the main reason for the low carbonation yield via direct moist carbonation of activated lizardite.

Both activation and carbonation conditions should be optimized to increase the proportion of highly relative to poorly-reactive amorphous Mg-rich silicate phases, as well as to avoid undesired side reactions in order to unlock (if possible) the direct carbonation potential of activated lizardite. If such a process cannot be significantly further optimized, such as increasing the proportion of HRAS relative to PRAS during activation of lizardite, other routes for the carbonation of lizardite should be considered such as indirect carbonation processes of both activated and non-activated lizardite.

ACKNOWLEDGEMENTS

This work has been partially funded by the Government of Catalonia through the FI-2017 program for the recruitment of early-stage researchers (K.R.). Contract number: 2017 FI_B00129 (K.R.). Authors are grateful to Prof. Joaquín Proenza (Universitat de Barcelona) who kindly provided the samples studied in this research. The authors gratefully acknowledge Prof. Alissa Park and Mr. Guanhi Rim for insightful discussions. Technical assistance in sample characterization of the reaction products by Drs. Trifon Trifonov and Montserrat Domínguez-Escalante, from the Barcelona Research Center in Multiscale Science and Engineering. Drs Jorge Molinero and Andrés Idiart from Amphos[21] Consulting S.L. España are gratefully acknowledged for their collaboration in the framework of the InnoEnergy PhD mobility program funding to A.C.

552 REFERENCES

553 Assima, G.P., Larachi, F., Beaudoin, G., Molson, J.W., 2012. CO_2 sequestration in chrysotile
554 mining residues - Implication of watering and passivation under environmental conditions
555 CO_2 sequestration in chrysotile mining residues - Implication of watering and passivation
556 under environmental co. Ind. Eng. Chem. Res. 51, 8726–8734.
557 https://doi.org/10.1021/ie202693q

558 Béarat, H., Mckelvy, M.J., Chizmeshya, A.V.G., Gormley, D., Nunez, R., Carpenter, R.W.,
559 Squires, K., Wolf, G.H., 2006. Carbon sequestration via aqueous olivine mineral carbonation:
560 Role of passivating layer formation. Environ. Sci. Technol. 40, 4802–4808.

561 Benhelal, E., Oliver, T.K., Farhang, F., Hook, J.M., Rayson, M.S., Brent, G.F., Stockenhuber, M.,
562 Kennedy, E.M., 2019a. Structure of Silica Polymers and Reaction Mechanism for Formation
563 of Silica-Rich Precipitated Phases in Direct Aqueous Carbon Mineralization. Ind. Eng. Chem.
564 Res. https://doi.org/10.1021/acs.iecr.9b04379

565 Benhelal, E., Rashid, M.I., Rayson, M.S., Brent, G.F., Oliver, T., Stockenhuber, M., Kennedy,
566 E.M., 2019b. Direct aqueous carbonation of heat activated serpentine: Discovery of
567 undesirable side reactions reducing process efficiency. Appl. Energy 242, 1369–1382.
568 https://doi.org/10.1016/j.apenergy.2019.03.170

569 Benhelal, E., Rashid, M.I., Rayson, M.S., Prigge, J.D., Molloy, S., Brent, G.F., Cote, A.,
570 Stockenhuber, M., Kennedy, E.M., 2018. Study on mineral carbonation of heat activated
571 lizardite at pilot and laboratory scale. J. CO2 Util. 26, 230–238.
572 https://doi.org/10.1016/j.jcou.2018.05.015

573 Bhardwaj, R., Van Ommen, J.R., Nugteren, H.W., Geerlings, H., 2016. Accelerating Natural CO_2
574 Mineralization in a Fluidized Bed. Ind. Eng. Chem. Res. 55, 2946–2951.
575 https://doi.org/10.1021/acs.iecr.5b04925

576 Blue, C.R., Giuffre, A., Mergelsberg, S., Han, N., De Yoreo, J.J., Dove, P.M., 2017. Chemical and
577 physical controls on the transformation of amorphous calcium carbonate into crystalline
578 $CaCO_3$ polymorphs. Geochim. Cosmochim. Acta 196, 179–196.

https://doi.org/10.1016/j.gca.2016.09.004

Bobicki, E.R., Liu, Q., Xu, Z., Zeng, H., 2012. Carbon capture and storage using alkaline industrial wastes. Prog. Energy Combust. Sci. 38, 302–320. https://doi.org/10.1016/j.pecs.2011.11.002

Canterford, J., Tsambourakis, G., Lambert, B., 1984. Some observations on the properties of dypingite, $Mg_5(CO_3)_4(OH)_2 \cdot 5H_2O$, and related minerals. Mineral. Mag. 48, 437–442.

Casey, W.H., Westrich, H.R., Arnold, G.W., 1988. Surface chemistry of labradorite feldspar reacted with aqueous solutions at pH = 2, 3, and 12. Geochim. Cosmochim. Acta 52, 2795–2807. https://doi.org/https://doi.org/10.1016/0016-7037(88)90147-0

Chizmeshya, A.V.G., Mckelvy, M.J., Sharma, R., Carpenter, R.W., Bearat, H., 2002. Density functional theory study of the decomposition of $Mg(OH)_2$: a lamellar dehydroxylation model. Mater. Chem. Phys. 77, 416–425.

Chizmeshya, A.V.G., McKelvy, M.J., Wolf, G.H., Carpenter, R.W., Gormley, D., Diefenbacher, J., Marzke, R., 2006. Enhancing the atomic-level understanding of CO2 mineral sequestration mechanisms via advanced computational modeling.

Daval, D., Sissmann, O., Menguy, N., Saldi, G.D., Guyot, F., Martinez, I., Corvisier, J., Garcia, B., Machouk, I., Knauss, K.G., Hellmann, R., 2011. Influence of amorphous silica layer formation on the dissolution rate of olivine at 90°C and elevated pCO2. Chem. Geol. 284, 193–209. https://doi.org/https://doi.org/10.1016/j.chemgeo.2011.02.021

Davies, P.J., Bubela, B., 1973. The transformation of nesquehonite into hydromagnesite. Chem. Geol. 12, 289–300. https://doi.org/10.1016/0009-2541(73)90006-5

Deelman, J.C., 2001. Breaking Ostwald's Rule. Chemie der Erde 61, 224–235.

Dlugogorski, B.Z., Balucan, R.D., 2014. Dehydroxylation of serpentine minerals: Implications for mineral carbonation. Renew. Sustain. Energy Rev. 31, 353–367. https://doi.org/10.1016/j.rser.2013.11.002

Du Breuil, C., Pasquier, L.C., Dipple, G., Blais, J.F., Iliuta, M.C., Mercier, G., 2019. Mineralogical

transformations of heated serpentine and their impact on dissolution during aqueous-phase mineral carbonation reaction in flue gas conditions. Minerals 9, 1–14. https://doi.org/10.3390/min9110680

Dufaud, F., Martinez, I., Shilobreeva, S., 2009. Experimental study of Mg-rich silicates carbonation at 400 and 500 °C and 1 kbar. Chem. Geol. 265, 79–87. https://doi.org/10.1016/j.chemgeo.2009.01.026

Edwards, H.G.M., Villar, S.E.J., Jehlicka, J., Munshi, T., 2005. FT-Raman spectroscopic study of calcium-rich and magnesium-rich carbonate minerals. Spectrochim. Acta - Part A Mol. Biomol. Spectrosc. 61, 2273–2280. https://doi.org/10.1016/j.saa.2005.02.026

Eloneva, S., Said, A., Fogelholm, C., Zevenhoven, R., 2012. Preliminary assessment of a method utilizing carbon dioxide and steelmaking slags to produce precipitated calcium carbonate. Appl. Energy 90, 329–334. https://doi.org/10.1016/j.apenergy.2011.05.045

Fagerlund, J., Highfield, J., Zevenhoven, R., 2012. Kinetics studies on wet and dry gas – solid carbonation of MgO and $Mg(OH)_2$ for CO_2 sequestration. RSC Adv. 10380–10393. https://doi.org/10.1039/c2ra21428h

Farhang, F., Oliver, T.K., Rayson, M., Brent, G., Stockenhuber, M., Kennedy, E., 2016. Experimental study on the precipitation of magnesite from thermally activated serpentine for CO_2 sequestration. Chem. Eng. J. 303, 439–449. https://doi.org/10.1016/j.cej.2016.06.008

Farhang, F., Rayson, M., Brent, G., Hodgins, T., Stockenhuber, M., Kennedy, E., 2017. Insights into the dissolution kinetics of thermally activated serpentine for CO_2 sequestration. Chem. Eng. J. 330, 1174–1186. https://doi.org/10.1016/j.cej.2017.08.073

Fauth, D.J., Baltrus, J.P., Soong, Y., Knoer, J.P., Howard, B.H., Graham, W.J., Maroto-Valer, M.M., Andrésen, J.M., 2002. Carbon Storage and Sequestration as Mineral Carbonates, in: Maroto-Valer, M.M., Song, C., Soong, Y. (Eds.), Environmental Challenges and Greenhouse Gas Control for Fossil Fuel Utilization in the 21st Century. Springer US, Boston, MA, pp. 101–117. https://doi.org/10.1007/978-1-4615-0773-4_8

Felmy, A.R., Qafoku, O., Arey, B.W., Hu, J.Z., Hu, M., Schaef, H.T., Ilton, E.S., Hess, N.J.,

Pearce, C.I., Feng, J., Rosso, K.M., 2012. Reaction of water-saturated supercritical CO_2 with forsterite : Evidence for magnesite formation at low temperatures. Geochim. Cosmochim. Acta 91, 271–282. https://doi.org/10.1016/j.gca.2012.05.026

Fricker, K.J., Park, A.A., 2013. Effect of H_2O on $Mg(OH)_2$ carbonation pathways for combined CO_2 capture and storage. Chem. Eng. Sci. 100, 332–341. https://doi.org/10.1016/j.ces.2012.12.027

Fricker, K.J., Park, A.H.A., 2014. Investigation of the different carbonate phases and their formation kinetics during $Mg(OH)_2$ slurry carbonation. Ind. Eng. Chem. Res. 53, 18170–18179. https://doi.org/10.1021/ie503131s

Frost, R.L., 2011. Raman spectroscopic study of the magnesium carbonate mineral hydromagnesite (Mg 5[(CO 3) 4(OH) 2]·4H 2O). J. Raman Spectrosc. 42, 1690–1694. https://doi.org/10.1002/jrs.2917

Fukushi, K., Suzuki, Y., Kawano, J., Ohno, T., Ogawa, M., Yaji, T., Takahashi, Y., 2017. Speciation of magnesium in monohydrocalcite: XANES, ab initio and geochemical modeling. Geochim. Cosmochim. Acta 213, 457–474. https://doi.org/10.1016/j.gca.2017.06.040

Gadikota, G., Matter, J., Kelemen, P., Park, A.A., 2014. Chemical and morphological changes during olivine carbonation for CO_2 storage in the presence of NaCl and $NaHCO_3$. Phys. Chem. Chem. Phys. 16, 4679. https://doi.org/10.1039/c3cp54903h

Gerdemann, S.J., O'Connor, W.K., Dahlin, D.C.D.C., Penner, L.R., Rush, H., O'Conor, W.K., Dahlin, D.C.D.C., Penner, L.R., Rush, H., 2007. Ex situ aqueous mineral carbonation. Environ. Sci. Technol. 41, 2589–2593. https://doi.org/10.1021/es0619253

Giammar, D.E., Bruant, R.G., Peters, C.A., 2005. Forsterite dissolution and magnesite precipitation at conditions relevant for deep saline aquifer storage and sequestration of carbon dioxide. Chem. Geol. 217, 257–276. https://doi.org/10.1016/j.chemgeo.2004.12.013

Hänchen, M., Prigiobbe, V., Baciocchi, R., Mazzotti, M., 2008. Precipitation in the Mg-carbonate system—effects of temperature and CO_2 pressure. Chem. Eng. Sci. 63, 1012–1028. https://doi.org/10.1016/J.CES.2007.09.052

Hao, Z., Du, F., 2009. Synthesis of basic magnesium carbonate microrods with a “house of cards” surface structure using rod-like particle template. J. Phys. Chem. Solids 70, 401–404. https://doi.org/10.1016/j.jpcs.2008.11.005

Harrison, A.L., Power, I.M., Dipple, G.M., 2013. Accelerated carbonation of brucite in mine tailings for carbon sequestration. Environ. Sci. Technol. 47, 126–134. https://doi.org/10.1021/es3012854

Hellmann, R., Eggleston, C.M., Hochella, M.F., Crerar, D.A., 1990. The formation of leached layers on albite surfaces during dissolution under hydrothermal conditions. Geochim. Cosmochim. Acta 54, 1267–1281. https://doi.org/https://doi.org/10.1016/0016-7037(90)90152-B

Highfield, J., Chen, J., Haghighatlari, M., Abacka, J., Zevenhoven, R., 2016. Low-temperature gas-solid carbonation of magnesia and magnesium hydroxide promoted by non-immersive contact with water. RSC Adv. 6, 89655–89664. https://doi.org/10.1039/C6RA16328A

Hopkinson, L., Kristova, P., Rutt, K., Cressey, G., 2012. Phase transitions in the system MgO-CO_2-H_2O during CO_2 degassing of Mg-bearing solutions. Geochim. Cosmochim. Acta 76, 1–13. https://doi.org/10.1016/j.gca.2011.10.023

Hopkinson, L., Rutt, K., Cressey, G., 2008. The Transformation of Nesquehonite to Hydromagnesite in the System CaO-MgO-H 2O-CO2 : An Experimental Spectroscopic Study. J. Geol. 116, 387–400. https://doi.org/10.1086/588834

Hövelmann, J., Putnis, C. V., Ruiz-Agudo, E., Austrheim, H., 2012. Direct nanoscale observations of CO_2 sequestration during brucite [$Mg(OH)_2$] dissolution. Environ. Sci. Technol. 46, 5253–5260. https://doi.org/10.1021/es300403n

Huijgen, W.J.J., Comans, R.N.J., Witkamp, G.J., 2007. Cost evaluation of CO_2 sequestration by aqueous mineral carbonation. Energy Convers. Manag. 48, 1923–1935. https://doi.org/10.1016/j.enconman.2007.01.035

Julcour, C., Bourgeois, F., Bonfils, B., Benhamed, I., Guyot, F., Bodénan, F., Petiot, C., Gaucher, É.C., 2015. Development of an attrition-leaching hybrid process for direct aqueous mineral

carbonation. Chem. Eng. J. 262, 716–726. https://doi.org/10.1016/j.cej.2014.10.031

Kelemen, P.B., Matter, J., 2008. In situ carbonation of peridotite for CO_2 storage. Proc. Natl. Acad. Sci. U. S. A. 105, 17295–17300. https://doi.org/10.1073/pnas.0805794105

Lackner, K.S., 2003. A Guide to CO_2 Sequestration. Science (80-.). 300, 1677–1678.

Lackner, K.S., Wendt, C.H., Butt, D.P., Joyce, E.L., Sharp, D.H., 1995. Carbon dioxide disposal in carbonate minerals. Energy 20, 1153–1170. https://doi.org/10.1016/0360-5442(95)00071-N

Lafay, R., Montes-Hernandez, G., Janots, E., Chiriac, R., Findling, N., Toche, F., 2014. Simultaneous precipitation of magnesite and lizardite from hydrothermal alteration of olivine under high-carbonate alkalinity. Chem. Geol. 368, 63–75. https://doi.org/10.1016/j.chemgeo.2014.01.008

Larachi, F., Daldoul, I., Beaudoin, G., 2010. Fixation of CO_2 by chrysotile in low-pressure dry and moist carbonation: Ex-situ and in-situ characterizations. Geochim. Cosmochim. Acta 74, 3051–3075. https://doi.org/10.1016/J.GCA.2010.03.007

Li, J., Hitch, M., Power, I.M., Pan, Y., 2018. Integrated mineral carbonation of ultramafic mine deposits—A review. Minerals 8, 1–18. https://doi.org/10.3390/min8040147

Li, Wenzhi, Li, Wen, Li, B., Bai, Z., 2009. Electrolysis and heat pretreatment methods to promote CO_2 sequestration by mineral carbonation. Chem. Eng. Res. Des. 87, 210–215. https://doi.org/10.1016/j.cherd.2008.08.001

Linga, P., Kumar, R., Englezos, P., 2007. The Clathrate Hydrate Process for Post and Pre-combustion Capture of Carbon Dioxide. J. Hazard. Mater. 149, 625–629. https://doi.org/10.1016/j.jhazmat.2007.06.086

Loring, J.S., Thompson, C.J., Zhang, C., Wang, Z., Schaef, H.T., Rosso, K.M., 2012. In situ infrared spectroscopic study of brucite carbonation in dry to water-saturated supercritical carbon dioxide. J. Phys. Chem. A 116, 4768–77. https://doi.org/10.1021/jp210020t

Mann, J., 2014. Serpentine Activation for CO2 Sequestration. Thesis Diseration. The University of Sideny.

Marchesi, C., Garrido, C.J., Proenza, J.A., Hidas, K., Varas-Reus, M.I., Butjosa, L., Lewis, J.F., 2016. Geochemical record of subduction initiation in the sub-arc mantle: Insights from the Loma Caribe peridotite (Dominican Republic). Lithos 252–253, 1–15. https://doi.org/10.1016/j.lithos.2016.02.009

Maroto-Valer, M.M., Fauth, D.J., Kuchta, M.E., Zhang, Y., Andrésen, J.M., 2005. Activation of magnesium rich minerals as carbonation feedstock materials for CO_2 sequestration. Fuel Process. Technol. 86, 1627–1645. https://doi.org/10.1016/j.fuproc.2005.01.017

McKelvy, M.J., Chizmeshya, A.V.G., Diefenbacher, J., Béarat, H., Wolf, G., 2004. Exploration of the role of heat activation in enhancing serpentine carbon sequestration reactions. Environ. Sci. Technol. 38, 6897–6903. https://doi.org/10.1021/es049473m

Montes-Hernandez, G., Renard, F., Chiriac, R., Findling, N., Toche, F., 2012. Rapid precipitation of magnesite from $Mg(OH)_2$-H_2O-CO_2 slurry enhanced by NaOH and heat-ageing step (from 20 to 90°C). Cryst. Growth Des. 12, 5233–5240.

Morse, J., Casey, W., 1988. Ostwald processes and mineral paragenesis in sediments. Am. J. Sci. 288, 537–560.

Mouedhen, I., Kemache, N., Pasquier, L.C., Cecchi, E., Blais, J.F., Mercier, G., 2017. Effect of pCO2 on direct flue gas mineral carbonation at pilot scale. J. Environ. Manage. 198, 1–8. https://doi.org/10.1016/j.jenvman.2017.04.048

Park, A.-H.A., Fan, L.-S., 2004. CO_2 mineral sequestration: physically activated dissolution of serpentine and pH swing process. Chem. Eng. Sci. 59, 5241–5247. https://doi.org/10.1016/J.CES.2004.09.008

Pasquier, L.C., Mercier, G., Blais, J.F., Cecchi, E., Kentish, S., 2014. Reaction mechanism for the aqueous-phase mineral carbonation of heat-activated serpentine at low temperatures and pressures in flue gas conditions. Environ. Sci. Technol. 48, 5163–5170. https://doi.org/10.1021/es405449v

737 Power, I.M., Dipple, G.M., Bradshaw, P.M.D., Harrison, A.L., 2020. Prospects for CO2
738 mineralization and enhanced weathering of ultramafic mine tailings from the Baptiste nickel
739 deposit in British Columbia, Canada. Int. J. Greenh. Gas Control 94, 102895.
740 https://doi.org/10.1016/j.ijggc.2019.102895

741 Power, I.M., Dipple, G.M., Southam, G., 2010. Bioleaching of ultramafic tailings by
742 Acidithiobacillus spp. for CO_2 sequestration. Environ. Sci. Technol. 44, 456–462.
743 https://doi.org/10.1021/es900986n

744 Power, I.M., Harrison, A.L., Dipple, G.M., 2016. Accelerating Mineral Carbonation Using
745 Carbonic Anhydrase. Environ. Sci. Technol. 50, 2610–2618.
746 https://doi.org/10.1021/acs.est.5b04779

747 Power, I.M., Harrison, A.L., Dipple, G.M., Wilson, S., Kelemen, P.B., Hitch, M., Southam, G.,
748 2013. Carbon Mineralization : From Natural Analogues to Engineered Systems From Natural
749 Analogues to Engineered Systems. Rev. Mineral. Geochemistry.
750 https://doi.org/10.2138/rmg.2013.77.9

751 Power, I.M., Harrison, A.L., Dipple, G.M., Wilson, S.A., Barker, S.L.L., Fallon, S.J., 2019.
752 Magnesite formation in playa environments near Atlin, British Columbia, Canada. Geochim.
753 Cosmochim. Acta 255, 1–24. https://doi.org/10.1016/j.gca.2019.04.008

754 Prigiobbe, V., Hänchen, M., Werner, M., Baciocchi, R., Mazzotti, M., 2009. Mineral carbonation
755 process for CO2 sequestration. Energy Procedia 1, 4885–4890.
756 https://doi.org/10.1016/j.egypro.2009.02.318

757 Prigiobbe, V., Mazzotti, M., 2013. Precipitation of Mg-carbonates at elevated temperature and
758 partial pressure of CO_2. Chem. Eng. J. 223, 755–763.
759 https://doi.org/10.1016/j.cej.2013.03.033

760 Pronost, J., Beaudoin, G., Lemieux, J.M., Hébert, R., Constantin, M., Marcouiller, S., Klein, M.,
761 Duchesne, J., Molson, J.W., Larachi, F., Maldague, X., 2012. CO_2-depleted warm air venting
762 from chrysotile milling waste (Thetford Mines, Canada): Evidence for in-situ carbon capture
763 from the atmosphere. Geology 40, 275–278. https://doi.org/10.1130/G32583.1

764 Rausis, K., Ćwik, A., Casanova, I., 2020. Phase evolution during accelerated CO_2 mineralization
765 of brucite under concentrated CO_2 and simulated flue gas conditions. J. CO2 Util. 37, 122–
766 133. https://doi.org/10.1016/j.jcou.2019.12.007

767 Rigopoulos, I., Petallidou, K.C., Vasiliades, M.A., Delimitis, A., Ioannou, I., Efstathiou, A.M.,
768 Kyratsi, T., 2015. Carbon Dioxide storage in Olivine Basalts : Effect of Ball Milling Process.
769 Powder Technol. 273, 220–229. https://doi.org/10.1016/j.powtec.2014.12.046

770 Sanna, A., Hall, M.R., Maroto-Valer, M., 2012. Post-processing pathways in carbon capture and
771 storage by mineral carbonation (CCSM) towards the introduction of carbon neutral materials.
772 Energy Environ. Sci. 5, 7781. https://doi.org/10.1039/c2ee03455g

773 Schaef, H., McGrail, B., Loring, J., Bowden, M., Arey, B., Rosso, K.M., 2013. Forsterite
774 [Mg_2SiO_4] Carbonation in wet supercritical CO_2: An in Situ High-Pressure X-ray Diffraction
775 Study. Environ. Sci. Technol. 47, 174–181.

776 Sipilä, J., Teir, S., Zevenhoven, R., 2008. Carbon Dioxide Sequestration by Mineral Carbonation :
777 Literature Review Update 2005-2007, Report for Faculty of Technology Heat Engineering
778 Laboratory. Turku, Finland.

779 Swanson, E.J., Fricker, K.J., Sun, M., Park, A.H.A., 2014. Directed precipitation of hydrated and
780 anhydrous magnesium carbonates for carbon storage. Phys. Chem. Chem. Phys. 16, 23440–
781 23450. https://doi.org/10.1039/c4cp03491k

782 Taifan, W., Boily, J., Baltrusaitis, J., 2016. Surface chemistry of carbon dioxide revisited. Surf.
783 Sci. Rep. 71, 595–671. https://doi.org/10.1016/j.surfrep.2016.09.001

784 Thom, J.G.M., Dipple, G.M., Power, I.M., Harrison, A.L., 2013. Chrysotile dissolution rates:
785 Implications for carbon sequestration. Appl. Geochemistry 35, 244–254.
786 https://doi.org/10.1016/j.apgeochem.2013.04.016

787 Tran, T.N., Pham, T.V.A., Le, M.L.P., Nguyen, T.P.T., Tran, V.M., 2013. Synthesis of amorphous
788 silica and sulfonic acid functionalized silica used as reinforced phase for polymer electrolyte
789 membrane. Adv. Nat. Sci. Nanosci. Nanotechnol. 4. https://doi.org/10.1088/2043-
790 6262/4/4/045007

Turvey, C.C., Wilson, S.A., Hamilton, J.L., Tait, A.W., McCutcheon, J., Beinlich, A., Fallon, S.J., Dipple, G.M., Southam, G., 2018. Hydrotalcites and hydrated Mg-carbonates as carbon sinks in serpentinite mineral wastes from the Woodsreef chrysotile mine, New South Wales, Australia: Controls on carbonate mineralogy and efficiency of CO2 air capture in mine tailings. Int. J. Greenh. Gas Control 79, 38–60. https://doi.org/10.1016/j.ijggc.2018.09.015

Veetil, S.P., Pasquier, L., Blais, J., 2015. Direct gas – solid carbonation of serpentinite residues in the absence and presence of water vapor : a feasibility study for carbon dioxide sequestration. Environ. Sci. Pollut. Res. 22, 13486–13495. https://doi.org/10.1007/s11356-015-4580-x

Werner, M., Hariharan, S., Mazzotti, M., 2014. Flue gas CO2 mineralization using thermally activated serpentine: From single- to double-step carbonation. Phys. Chem. Chem. Phys. 16, 24978–24993. https://doi.org/10.1039/c4cp02786h

Werner, M., Hariharan, S.B., Bortolan, A. V., Zingaretti, D., Baciocchi, R., Mazzotti, M., 2013. Carbonation of activated serpentine for direct flue gas mineralization. Energy Procedia 37, 5929–5937. https://doi.org/10.1016/j.egypro.2013.06.519

Wilson, S.A., Harrison, A.L., Dipple, G.M., Power, I.M., Barker, S.L.L., Ulrich Mayer, K., Fallon, S.J., Raudsepp, M., Southam, G., 2014. Offsetting of CO_2 emissions by air capture in mine tailings at the Mount Keith Nickel Mine, Western Australia: Rates, controls and prospects for carbon neutral mining. Int. J. Greenh. Gas Control 25, 121–140. https://doi.org/10.1016/j.ijggc.2014.04.002

Zarandi, A., Larachi, F., Beaudoin, G., Plante, B., Sciortino, M., 2017a. Ambient mineral carbonation of different lithologies of mafic to ultramafic mining wastes/tailings – A comparative study. Int. J. Greenh. Gas Control 63, 392–400. https://doi.org/10.1016/j.ijggc.2017.06.016

Zarandi, A., Larachi, F., Beaudoin, G., Plante, B., Sciortino, M., 2017b. Nesquehonite as a carbon sink in ambient mineral carbonation of ultramafic mining wastes. Chem. Eng. J. 314, 160–168. https://doi.org/10.1016/j.cej.2017.01.003

Zevenhoven, R., Teir, S., Eloneva, S., 2008. Heat optimisation of a staged gas – solid mineral

carbonation process for long-term CO_2 storage. Energy 33, 362–370. https://doi.org/10.1016/j.energy.2007.11.005

Zhao, L., Sang, L., Jun, C., Ji, J., Teng, H.H., 2010. Aqueous carbonation of natural brucite: Relevance to CO_2 sequestration. Environ. Sci. Technol. 44, 406–411. https://doi.org/10.1021/es9017656

Zou, Z., Habraken, W.J.E.M., Matveeva, G., Jensen, A.C.S., Bertinetti, L., Hood, M.A., Sun, C., Gilbert, P.U.P.A., Polishchuk, I., Pokroy, B., Mahamid, J., Politi, Y., Weiner, S., Werner, P., Bette, S., Dinnebier, R., Kolb, U., Zolotoyabko, E., Fratzl, P., 2019. A hydrated crystalline calcium carbonate phase: Calcium carbonate hemihydrate. Science (80-.). 363, 396–400. https://doi.org/10.1126/science.aav0210